arXiv:astro-ph/0407046v1 2 Jul 2004

Analysis of *RGU* Photometry in Selected Area 51

S. Bilir[1]*, S. Karaali[1], and R. Buser[2]

March 20, 2022

[1]İstanbul University Science Faculty, Department of Astronomy and Space Sciences
34119 İstanbul-TURKEY
sbilir@istanbul.edu.tr
[2]Astronomisches Institut der Universität Basel, Venusstrasse 7
4102 Binningen-SWITZERLAND

Abstract

A low-latitude anticenter field ($l = 189°$, $b = +21°$) is investigated by using the full calibration tools of *RGU* photometry. The observed *RGU* data are reduced to the standard system and the separation of dwarfs and evolved stars is carried out by an empirical method. Stars are categorized into three metallicity classes, i.e. $-0.25 < [M/H] \leq +0.50$, $-1.00 < [M/H] \leq -0.25$, and $[M/H] \leq -1.00$ dex, and their absolute magnitudes are determined by the corresponding colour-magnitude diagrams. The unusually large scattering in the two-colour diagrams is reduced by excluding 153 extra-galactic objects, identifying them compared with the charts of Basel Astronomical Institute and University of Minnesota, and by the criterion and algorithm of Gaidos et al. [1]. The local logarithmic space density for giants, $D^*(0) = 6.75$, lies within the local densities of Gliese and Gliese & Jahreiss. The local luminosity function for the absolute magnitude interval $3 < M(G) \leq 7$ agrees with Hipparcos' better than Gliese's, whereas there is a considerable excess for the interval $7 < M(G) \leq 8$ relative to both luminosity functions. This discrepancy may be due to many reasons, i.e. cumulative catalogue errors, binarity etc.

Key Words: Galaxy: structure – Stars: luminosity function – Photometry: RGU

1 Introduction

Buser's [2] photographic *RGU* system is a systematic work based on synthetic photometry (Buser [3]). Galactic fields can be investigated through the method given by Buser & Fenkart [4], thus main-sequence stars can be separated into

*corresponding author

three categories, i.e. Thin Disk, Thick Disk, and Halo, with available absolute magnitudes and metallicities. Additionally the standardized catalogues for 14 fields, properly selected from Basel Halo Program are recently used for constructing a new Galactic model (Buser et al. [5, 6]). The lack of calibration of evolved stars (sub-giants and giants) in the work of Buser & Fenkart [4] is compensated by Buser et al. [7], but without giving a method for their separation.

While standard star count analysis provide a description of the present structure of the Galaxy, additional data such as kinematics and chemical abundance are required for understanding the formation and evolution of our Milky Way Galaxy. Although Buser's *RGU* photometry provides the metallicity distribution of field stars, it does not have an index suitable to the surface gravity, hence the separation of dwarfs (main-sequence stars) and evolved stars requires an indirect method (Karaali [8], Ak et al. [9], Karataş et al. [10], Karaali et al. [11], and Karataş et al. [12]).

The excess of the luminosity function for absolutely faint magnitudes, i.e. $M(G) > 6$ mag, had been used as a clue for such a separation in many works (Fenkart [13-16]) and apparently bright stars (roughly $G < 15 - 16$ mag) with $M(G) > 6$ mag on the main-sequence had been adopted as evolved stars with correspondingly brighter absolute magnitudes. A few iterations are sufficient to obtain a luminosity function agreeable with the luminosity functions of Gliese [17] and Hipparcos (Jahreiss & Wielen [18, JW]).

The comparison of Basel and Minnesota charts revealed that there is a considerable number of extra-galactic objects in the star fields, which cause an excess in the density and luminosity functions (Bilir et al. [19]). Hence, we applied the same procedure to eliminate such objects in our field. It turned out that 153 sources are extra-galactic objects, galaxies, occupying different regions in the two-colour diagrams. By adopting the *distances from the stellar locus* criterion and the algorithm of Gaidos et al. [1] (see also Newberg & Yanny [20]) however, with slight modification and purpose (see Section 3 for detail). Thus, recovery of the local luminosity function as given by Gliese [17] and/or Hipparcos (JW) could be possible. Section 2 is devoted to observations, reductions, and standardizations. Two-colour diagrams are given in Section 3, where the identification of extra-galactic objects, by comparison of the charts of Basel Astronomical Institute and Minnesota University, as well as the treatment of statistical scatter of stellar colours by means of criterion and algorithm of Gaidos et al. [1] is carried out. The separation of dwarfs and evolved stars and their absolute magnitude determination, and density and luminosity functions are given in Sections 4 and 5 respectively. Finally, summary and conclusion is presented in Section 6. We hope to derive the nature and distribution of stars in this field by applying the full calibration tools of *RGU* photometry.

2 Observations, Reductions, and Standardization

The coordinates of the field with size 0.45 square degrees are $\alpha = 07^h\ 28^m$, $\delta = +29^o\ 55'$; $l = 189^o$, $b = +21^o$ (1950). 1737 stars were measured by one

of us (S.K.) in 1995 at the Basel Astronomical Institute down to a apparent magnitude of $G = 19$ on each five plates for each band, i.e. R, G, and U. 50 stars photoelectrically measured by Purgathofer [21] with 19.00, 18.65, and 17.65 as faintest $U-$, $B-$, and $V-$ magnitudes have been used as standards and their UBV data were transformed to RGU-system by means of Buser's [22] formulae. The corresponding faintest $R-$, $G-$, and $U-$ magnitudes are 16.98, 18.25, and 20.09 respectively. The mean catalogue errors are given in Table 1. The $(U-B, B-V)$ two-colour diagram for standards reveals a colour-excess of $E(B-V) = 0^m.03$ which corresponds to $E(G-R) = 0^m.04$ in RGU (Buser [2]). This value is close to those of Schlegel et al. [23], $E(B-V) = 0^m.064$, and Burnstein & Heiles [24], $E(B-V) = 0^m.06$, who used different methods for their derivations, however. The first one is a model value, whereas the second one is derived from iso-obscuring contours with scale 0.03 mag.

ΔG versus $(G-R)_{obs}$ in Fig. 1a give no indication for a colour-equation for G, whereas there is a linear relation between ΔR versus $(G-R)_{obs}$, i.e. $\Delta R = -0.11(G-R)_{obs} + 0.14$ (Fig. 1b), and a step function between ΔU versus $(U-G)_{obs}$ (Fig. 1c) as follows, where Δm (m = G, R, and U) is the difference between the standard (m_s) and observed (m_{obs}) apparent magnitudes, and $(G-R)_{obs}$ and $(U-G)_{obs}$ are the observed colour-indices: $\Delta U = +0.08$, 0.00, -0.01, and +0.05 for $(U-G)_{obs} \leq 1.00$, $1.00 < (U-G)_{obs} \leq 1.65$, $1.65 < (U-G)_{obs} \leq 2.20$, and $2.20 < (U-G)_{obs}$, respectively.

All the RGU data are reduced to the standard system by applying the corrections mentioned above. Thus, all magnitudes and colours which will be used henceforth are dereddened and standard ones.

3 Two-Colour Diagrams

The two-colour diagrams are drawn within the limiting apparent magnitude of $G = 18$ for consecutive G- apparent magnitude intervals, where four of them, i.e. (14.0-15.0], (15.5-16.0], (16.5-17.0], and (17.5-18.0] are given in Fig. 2, respectively, as examples. As cited in Section 1, there is an unusually large scatter in these diagrams for low latitude field ($b = +21^o$), especially in the location of metal-poor stars in apparently faint magnitude intervals. The comparison of the charts of the Basel Astronomical Institute and Minnesota University reveals that 153 of 1737 objects are extra-galactic ones. However, omitting these objects does not reduce the scattering considerably, because they lie even within the region occupied by stars, i.e. $-3.0 < [M/H] < +0.5$ dex. The extra-galactic objects in the two-colour diagrams given in Fig. 2 are marked with a different symbol ($\triangle$).

The luminosity function for all stars (without extra-galactic objects) within the limiting apparent magnitude, $G = 18$, (Fig. 5b) resulting from the comparison of density functions with model gradients (see Section 5) Buser et al. [5, 6] (henceforth, BRK) deviates systematically from that of Gliese [17], i.e. there is an excess of absolutely faint stars, $M(G) > 6$, and deficience of absolutely bright stars, $M(G) < 5$, indicating that the scattering affected the absolutely bright stars to shift to the region of faint ones. It is worth noting that this is what we had experienced in our other works (cf. Fenkart & Karaali [25]).

We applied the *distances from the stellar locus* criterion and the algorithm of Gaidos et al. [1] (see also Newberg & Yanny [20]) with a slight modification and purpose, however, to reduce the number of scattered stars. These authors formed a locus of all pointlike sources in the multi-colour space and they fitted a set of locus points along the center of the locus of these sources. The stellar candidates selected were those that were closer to their associated locus point than the metric distance d (a parameter to be determined) in magnitudes for all colours, whereas the quasi-stellar object candidates were the ones at distances larger than d. In our case, we applied this criterion and algorithm to the colour-plane, i.e. $(U-G, G-R)$ two-colour diagram, and adopted the metric distance as $d = 1.3s$, where s is the standard deviation for each colour, for each sub-sample of stars (separated by dashed lines in Fig. 3b). Thus, stars for each sub-sample, within at least $1s$ were included in the statistics (see Table 2 for their percentages). Fig. 3a gives all dwarfs in the field SA 51, and Fig. 3b those selected by the criterion and algorithm of Gaidos et al. [1]) for statistical purpose.

4 Dwarf-Giant Separation and Absolute Magnitude Determination

Dwarfs and late-type giants were separated by the gap-criterion (Becker [26]) for a long time, whereas no effort was carried out for the separation of sub-giants. Late-type giants were recognized by their location separated from dwarfs by a gap and with larger $U-G$ colour-indices relative to the main-sequence with $[M/H] \sim 0.0$ dex, in the $(U-G, G-R)$ two-colour diagrams for low-latitude fields (cf. Becker & Fang [27]; Hersperger [28]). However, Becker [29] showed that there exists another type of late-type giant, lying at the metal-poor region of the two-colour diagram, and a bit bluer than the ones mentioned above, thus a bit disregarding the gap which separates dwarfs and metal-rich late-type giants. During the epoch of comparison the density functions with the galactic models, the local logarithmic space density for late-type giants, i.e. $\odot = 6.64$ (Gliese [17]), was the favour clue for their separation (Del Rio & Fenkart [30]; Fenkart [13-16]; Fenkart & Karaali [25]).

Systematic deviation of the luminosity functions from the one of Gliese [17] revealed that the absolutely faint segment of the luminosity function was contaminated by evolved stars (sub-giants and giants), resulting in an excess for $M(G) > 6$ mag and a deficience for $M(G) < 5$ mag in the luminosity function. This disagreement was used as a clue for the separation of dwarfs and evolved stars in recent years (Karaali [8], Ak et al. [9], Karataş et al. [10], Karaali et al. [11], and Karataş et al. [12]). The fundamental assumption for this empirical method is that apparently bright and absolutely faint stars on the main-sequence are evolved. In this work, a few iterations provided a luminosity function in best agreement with the local luminosity function as given by Gliese [17] and/or Hipparcos (JW) by assuming that for apparent magnitudes brighter than $G = 15.5$ mag, stars which according to their positions in the two-colour diagram could be identified as dwarfs with assigned absolute magnitudes fainter than $M(G) = 6$ mag, are however most likely evolved stars with correspondingly

brighter absolute magnitudes.

Following Buser & Fenkart [4]; we separated dwarfs into three metallicity-classes, i.e. $-0.25 < [M/H] \leq +0.50$ dex (Thin Disk), $-1.00 < [M/H] \leq -0.25$ dex (Thick Disk), and $[M/H] \leq -1.00$ dex (Halo), and we used their corresponding colour-magnitude diagram, derived from extent sources via synthetic photometry, for absolute magnitude determination. Contrary to the works investigated in Steinlin's [31] system, individual absolute magnitudes are adopted for late-type giants (and sub-giants) by separating them into different metallicity-classes and using the multi-metallicity colour-magnitude diagram of Buser et al. [7], derived in the same way as dwarfs.

5 Density and Luminosity Functions

The logarithmic space densities $D^* = logD(r)+10$ are evaluated for five absolute magnitude intervals, i.e. (3-4], (4-5], (5-6], (6-7], and (7-8], where the absolute magnitudes are complete, and for late-type giants (Tables 3 and 4). However, the number of stars for the absolute magnitude intervals (2-3], (8-9], and (9-10] for each distance interval is also given in Table 3. Here $D = N/\Delta V_{1,2}$, N being the number of stars, found in the partial volume $\Delta V_{1,2}$ which is determined by its limiting distances r_1 and r_2, and by the apparent field size in square degrees A, i.e. $\Delta V_{1,2} = (\pi/180)^2(A/3)(r_2^3 - r_1^3)$.

The density functions are most appropriately given in the form of histograms whose sections with ordinates $D^*(r_1, r_2)$ cover the distance-intervals (r_1, r_2), and heavy dots on the histogram sections $D^*(r_1, r_2)$ designate the centroid-distance $\bar{r} = [(r_1^3+r_2^3)/2]^{1/3}$ of the corresponding partial volume $\Delta V_{1,2}$ (Del Rio & Fenkart [30]; Fenkart & Karaali [25]; and Fenkart [13-16]).

The density functions are compared with the galactic model of BRK, in the form $\Delta logD(r) = logD(r, l, b) - logD(0, l, b)$ versus r, where $\Delta logD(r)$ is the difference between the logarithmic densities at distance r and at the Sun. Thus, $\Delta logD(r) = 0$ points out the logarithmic space density for $r = 0$ which is available for local luminosity function determination. The comparison is carried out as explained in some works of Basel fields (Del Rio & Fenkart [30]; Fenkart & Karaali [25], i.e. by shifting the model curve perpendicular to the distance axis until the best fit to the histogram results at the centroid distances (Fig. 4).

Fig. 4 show that there is a good agreement between the model gradients and the observed density histograms. The same agreement holds when local densities are considered, except for the absolute magnitude interval $7 < M(G) \leq 8$. This can be confirmed by comparison of the local luminosity function with the luminosity function of Gliese [17] and Hipparcos (JW). In Fig. 5, there are two luminosity functions resulting from comparisons of observed density histograms for dwarfs and sub-giants with the best-fitting model gradients BRK. For (a) we used the data in Table 3 and Fig. 4a-e where unusual scattering in the two-colour diagrams is reduced by the criterion and algorithm of Gaidos et al. [1], whereas for (b) all dwarfs and sub-giants within the limiting apparent magnitude, $G = 18$, are used. The agreement is much better for (a). The luminosity (a) for the interval $5 < M(G) \leq 6$, is almost equal to those of Gliese and Hipparcos

and close to them for the interval $6 < M(G) \leq 7$, but it is a bit deficient relative to the luminosity function of Hipparcos for the segment $3 < M(G) \leq 5$ (the luminosity function of Hipparcos is also deficient relative to the luminosity function of Gliese for the same absolute magnitude interval). However, there is a considerable excess for the luminosity function (a) relative to both luminosity functions of Gliese and Hipparcos for the interval $7 < M(G) \leq 8$, i.e. 0.30 in units of logarithmic space density which is much larger than the standard deviation for this absolute magnitude interval (Table 5). It is worth noting to note that the differences between the luminosity function (a) and that of Hipparcos for other absolute magnitude intervals are all less than the corresponding standard deviations given in Table 5. Although the luminosity function (b) is close to the luminosity function (a) for the absolute magnitude intervals (3-4], (4-5], and (5-6], it deviates from (a) for two absolutely faint magnitude intervals, i.e. (6-7], and (7-8], considerably.

The comparison of the density function for giants with the model gradients BRK is carried out up to $r = 10$ kpc (Fig. 4f). Six stars within the large distance interval $10.00 < r \leq 19.95$ kpc are not included in the statistics. The local density resulting from this comparison, $D^*(0) = 6.75$, lies between the local densities of Gliese [17] and Gliese & Jahreiss [32], i.e. $\odot = 6.64$ and $\odot = 6.92$, respectively.

6 Summary and Conclusion

We used the full calibration tools of *RGU* photometry to investigate the low-latitude ($b = +21^o$) and anticenter ($l = 189^o$) field SA 51. The observed *RGU* data are reduced to the standard system and the separation of dwarfs and evolved stars is carried out by an empirical method based on the assumption that apparently bright stars are evolved (Karaali [8], Ak et al. [9], Karataş et al. [10], Karaali et al. [11], and Karataş et al. [12]), i.e. for apparent magnitudes brighter than $G = 15.5$ mag, stars which, according to their positions, are identified as dwarfs with assigned absolute magnitude fainter than $M(G) = 6$ mag, are however most likely evolved stars with corresponding brighter absolute magnitudes. This assumption provided a luminosity function agreeable with the local luminosity function as given by Gliese [17] and Hipparcos (JW). Dwarfs are separated into three metallicity classes, i.e. $-0.25 < [M/H] \leq +0.50$ dex (Thin Disk), $-1.00 < [M/H] \leq -0.25$ dex (Thick Disk), and $[M/H] \leq -1.00$ dex (Halo), and their absolute magnitudes are determined by the corresponding colour-magnitude diagrams of Buser & Fenkart [4], derived from extent sources via synthetic photometry. The metallicities and absolute magnitudes for evolved stars are evaluated by the recent diagrams of Buser et al. [7].

Although 153 extra-galactic objects were excluded from the complete sample, compared with the charts of Basel Astronomical Institute and Minnesota University (Bilir et al. [19]), the scattering in the two-colour diagrams could not be reduced. We applied the criterion and algorithm of Gaidos et al. [1] to the colour-plane, i.e. $(U-G, G-R)$ two-colour diagram, to reject dwarfs at distances in magnitude larger than $d = 1.3s$ from the center of the locus of all dwarfs in

the direction to $U-G$ and $G-R$ axes, where s is the standard deviation of dwarfs associated with the locus point in each sub-sample (separated by dashed lines in Fig. 3b). This limitation reduced dwarfs by 79% which is larger than the percentage in $1s$ for a gaussian distribution.

The density histograms for dwarfs and sub-giants with absolute magnitudes (3-4], (4-5], (5-6], (6-7], and (7-8] agree with the model gradients BRK. The same agreement holds when local densities are considered, except for the absolute magnitude interval $7 < M(G) \leq 8$ where the luminosity has an excess of 0.30 in units of logarithmic density relative to the luminosity of Hipparcos. The number of dwarfs in this interval can not be reduced, otherwise they turn out to be giants with density function contradicting with the model gradients BRK and local density different than the ones of Gliese [17] and Gliese & Jahreiss [32].

One of the reasons for the deviation of the luminosity function for the interval $7 < M(G) \leq 8$ from Gliese's [17] or Hipparcos' (JW) may be binarity, besides others such as cumulative catalogue errors etc. We refer to Buser & Kaeser [33], who were the first to consider the effects of unresolved stars in the far-field surveys and luminosity functions. It may require the comparison of the luminosity functions with an appropriately redetermined local one via the data of Gliese [17] or Hipparcos (JW).

The luminosity function in our work is much better than the one in Karataş et al. [10]. All the tools used for the investigation of two fields are the same, except the distance criterion and algorithm of Gaidos et al. [1] which is used only in our work. This new approach can be useful for understanding the nature of stars in the fields treated.

Acknowledgements: We would like to thank Schweizerischer Nationalfonds zur Förderung der Wissenschaflichen Forschung, and the Scientific and Technical Research Council of Turkey for financial support (TBAG-AY/74), and the University of Minnesota for providing us with its APS on-line catalogues for the investigated field.

References

[1] E. J. Gaidos, E. A. Magnier, & P. L. Schechter, *PASP,* **105,** (1993), 1294.

[2] R. Buser, *A&A,* **62,** (1978), 425.

[3] R. Buser, PhD. Thesis, Astronomisches Institut der Universität Basel, Switzerland, 1975.

[4] R. Buser, & R. P. Fenkart, *A&A,* **239,** (1990), 243.

[5] R. Buser, J. Rong, & S. Karaali, *A&A,* **331,** (1998), 934 (BRK).

[6] R. Buser, J. Rong, & S. Karaali, *A&A,* **348,** (1999), 98.

[7] R. Buser, Y. Karataş, Th. Lejeune, J. X. Rong, P. Westera, & S. G. Ak, *A&A,* **357,** (2000), 988.

[8] S. Karaali, VIII. Nat. Astron. Symp. Eds. Z. Aslan & O. Gölbaşı, Ankara-Turkey, (1992), p.202.

[9] S. G. Ak, S. Karaali, & R. Buser, *A&AS,* **131,** (1998), 345.

[10] Y. Karataş, S. Karaali, & R. Buser, *A&A,* **373,** (2001), 895

[11] S. Karaali, S. Bilir, & R. Buser, *PASA*, (2004) (accepted).

[12] Y. Karataş, S. Bilir, S. Karaali, & S. G. Ak, *AN*, (2004) (accepted).

[13] R. P. Fenkart, *A&AS,* **78,** (1989), 217.

[14] R. P. Fenkart, *A&AS,* **79,** (1989), 51.

[15] R. P. Fenkart, *A&AS,* **80,** (1989), 89.

[16] R. P. Fenkart, *A&AS,* **81,** (1989), 187.

[17] W. Gliese, Veröff. Astron. Rechen Inst. Heidelberg, (1969), No:22.

[18] H. Jahreiss, & R. Wielen, in: HIPPARCOS'97. Presentation of the HIPPARCOS and TYCHO catalogues and first astrophysical results of the Hippaccos space astrometry mission, B. Battrick, M. A. C. Perryman, & P. L. Bernacca, (eds.), ESA SP-402, Noordwÿk, (1997), p.675 (JW).

[19] S. Bilir, Y. Karataş, & S. G. Ak, *TJPh,* **27,** (2003), 235.

[20] H. J. Newberg, & B. Yanny, *ApJS,* **113,** (1997), 89.

[21] A. Th. Purgathofer, *Bulletin/Lowell Observatory,* **7,** (1969), No: 147, p.98.

[22] R. Buser, in, Fresneau A., Hamm M. (eds.) Impacts des surveys du visible sur notre connaissance de la Galaxie. Comptes rendus sur les Journees de Strasbourg, 9eme Reunion, Obs. de Strasbourg, (1988), p.15.

[23] D. J. Schlegel, D. P. Finkbeiner, & M. Davis, *ApJ,* **500,** (1998) 525.

[24] D. Burnstein, & C. Heiles, *AJ,* **87,** (1982), 1165.

[25] R. P. Fenkart, & S. Karaali, *A&AS,* **69,** (1987), 33.

[26] W. Becker, *ZA,* **54,** (1962), 155.

[27] W. Becker, & Ch. Fang, *A&A,* **22,** (1973), 187.

[28] Th. Hersperger, *A&A,* **22,** (1973), 195.

[29] W. Becker, *A&AS,* **38,** (1979), 341.

[30] G. Del Rio, & R. P. Fenkart, *A&AS,* **68,** (1987), 397.

[31] U. W. Steinlin, *ZA,* **69,** (1968), 276.

[32] W. Gliese, & H. Jahreiss, Third Catalogue of Nearby Stars (Preliminary Version), Astron. Rechen Inst. Heidelberg, (1992).

[33] R. Buser, & U. Kaeser, *A&A,* **145,** (1985), 1.

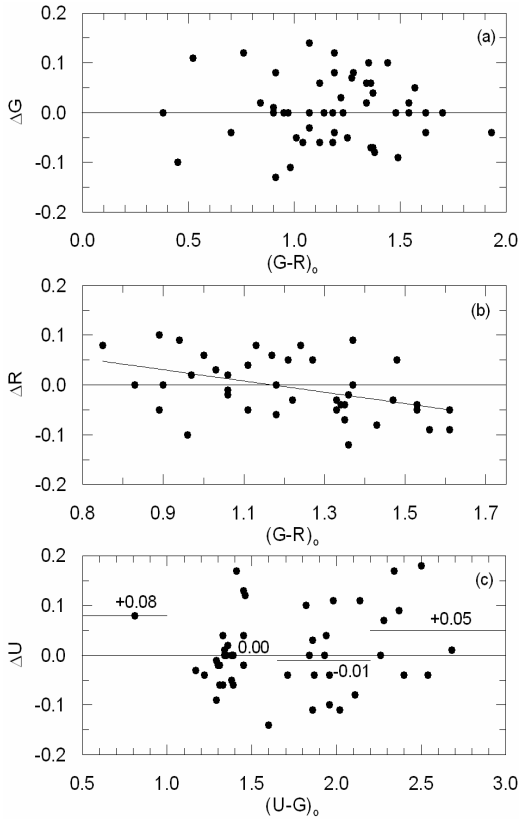


Figure 1: Standardization of the data. There is no indication for any colour - equation for G (a), whereas there is a linear relation between ΔR versus $(G-R)_{obs}$ (b), and a step function between ΔU versus $(U-G)_{obs}$ (c).

Table 1: Mean catalogue errors.

G interval	$(G)_{err}$	$(G-R)_{err}$	$(U-G)_{err}$
<12	± 0.02	± 0.02	± 0.03
(12-14]	0.02	0.02	0.03
(14-16]	0.02	0.03	0.02
>16	0.03	0.04	0.03

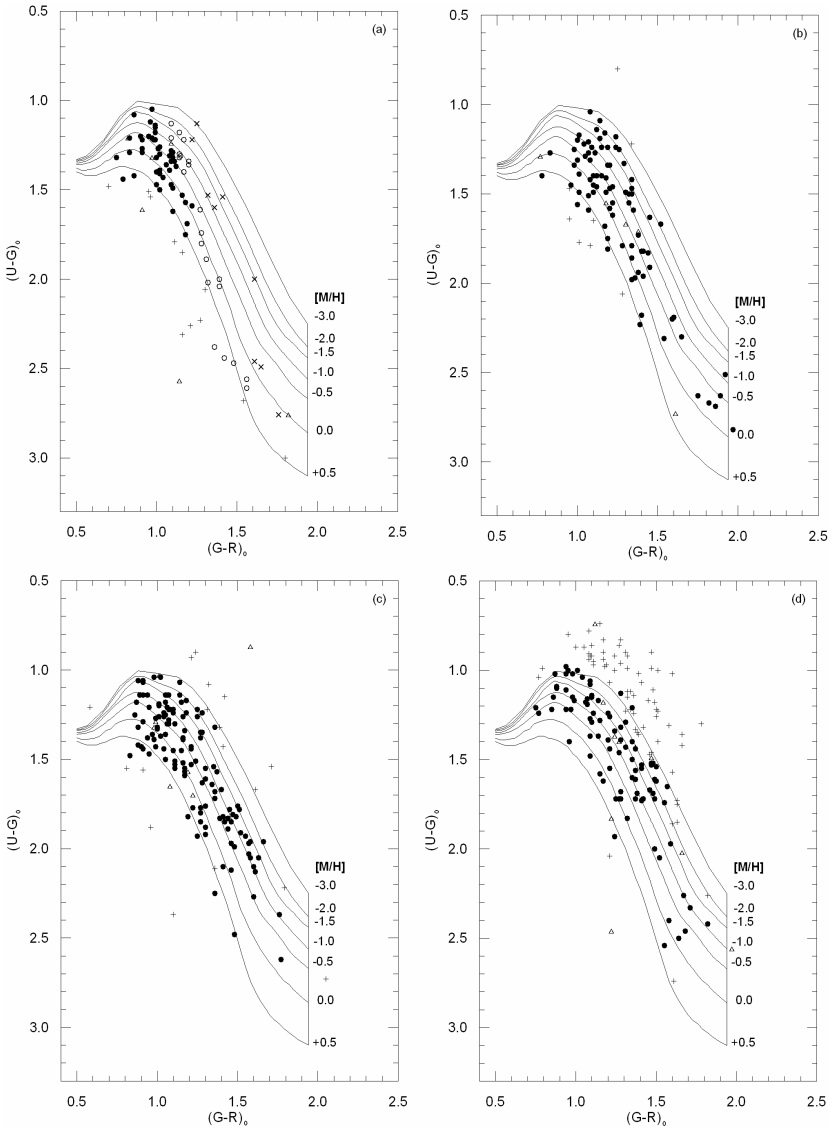


Figure 2: Four two-colour diagrams as examples, for (14.0-15.0] (a), (15.5-16.0] (b), (16.5-17.0] (c), and (17.5-18.0] (d). There is an unusually large scatter, especially in the faintest apparent magnitude interval, in the location of metal-poor stars. Symbols: (•) dwarfs, (o) sub-giants, (x) late-type giants, (△) extra-galactic objects, and (+) not included into statistics.

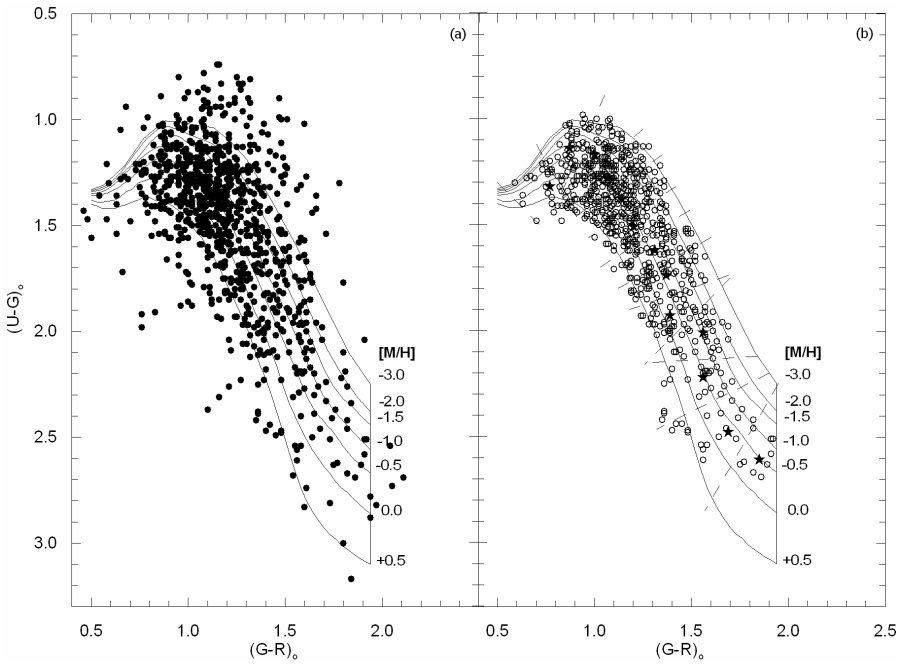


Figure 3: Two-colour diagram for dwarfs brighter than the apparently limiting magnitude, $G = 18$ mag. (a) for all stars, (b) for stars included into statistics, i.e. within the distance $d = 1.3s$, for $U - G$, and $G - R$ colours, from the corresponding locus point associated. The symbol ($\star$) denotes the locus point and the dashed lines separate dwarfs into sub-samples with centroid ($\star$). s: standard deviation for each colour, for the corresponding sub-sample.

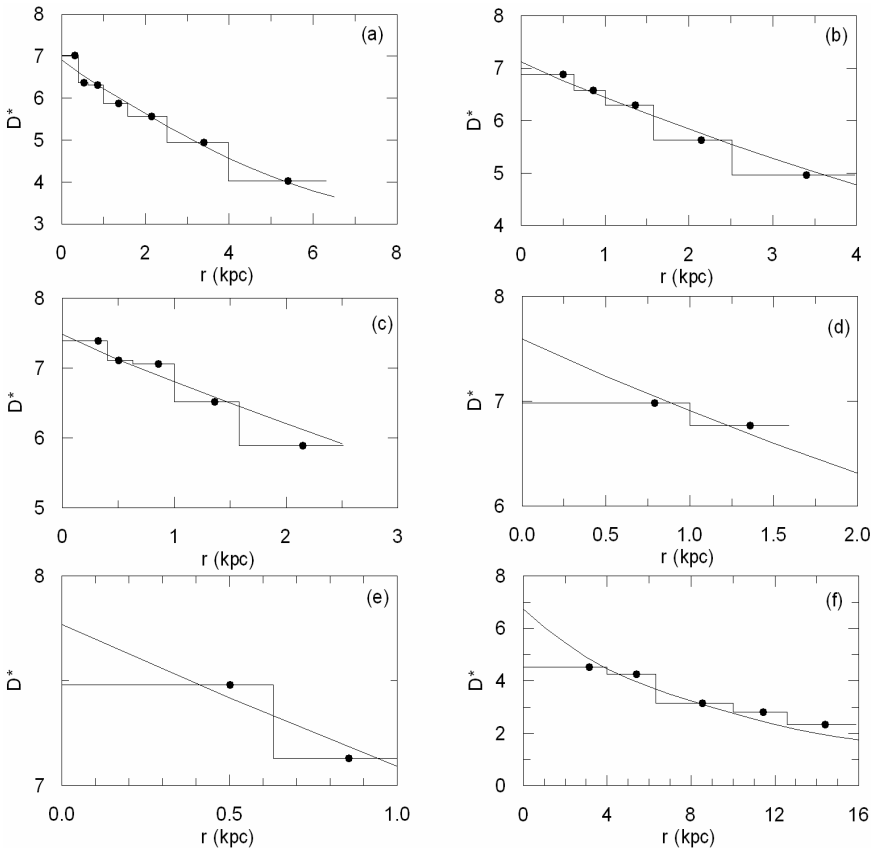


Figure 4: Logarithmic space-density histograms for dwarfs and sub-giants of different absolute-magnitude intervals: (3-4] (a), (4-5] (b), (5-6] (c), (6-7] (d), (7-8] (e), and for late-type giants (f). (•) centroid distance within the limiting distance of completeness, for comparison with model gradients BRK.

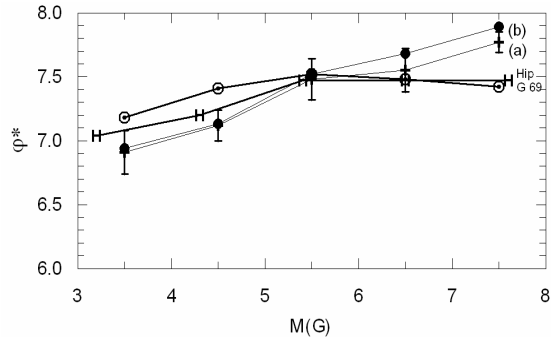


Figure 5: Two luminosity functions resulting from comparison of observed histograms with best-fitting model gradients BRK, and confronted to Gliese's [17] ($\odot$), and Hipparcos' [18] (H). (a) for dwarfs and sub-giants for which unusually scattering in the two-colour diagrams is reduced by the criterion and algorithm of Gaidos et al. [1] (taken from Table 3), and (b) for all dwarfs and sub-giants in the two-colour diagrams within the limiting apparent magnitude, $G = 18$ (the density functions for (b) have not been given to avoid space consuming).

Table 2: The $U - G$, $G - R$ colour-indices of the locus points (W), number of stars, for each sub-sample, associated with them ($N^{'}$) and within the distance $d = 1.3s$ from the corresponding locus point (N), and the percentage of stars included into statistics (s: standard deviation for each colour for the sub-sample considered).

W	$U-G$	$G-R$	$N^{'}$	N	%
1	1.32	0.77	30	20	67
2	1.14	0.87	50	41	82
3	1.17	1.00	107	76	71
4	1.28	1.07	146	133	91
5	1.38	1.14	144	108	75
6	1.51	1.20	100	81	81
7	1.62	1.31	67	53	79
8	1.74	1.37	81	62	77
9	1.93	1.39	53	41	77
10	2.01	1.56	38	29	76
11	2.22	1.56	25	18	72
12	2.48	1.69	22	19	86
13	2.61	1.85	10	8	80

Table 3: The logarithmic space densities $D^* = \log D + 10$ for five absolute magnitude intervals, i.e. (3-4], (4-5], (5-6], (6-7], and (7-8] for dwarfs and sub-giants, where the absolute magnitudes are complete. Thick horizontal lines: limiting distance of completeness (for definition of the symbols see text, distances in kpc, volumes in pc^3).

		$M(G) \rightarrow$	(2-3]	(3-4]	(4-5]	(5-6]	(6-7]	(7-8]	(8-9]	(9-10]
r_1-r_2	$\Delta V_{1,2}$	$\bar{r}$	N D*	N D*	N D*	N D*	N D*	N D*	N D*	N D*
0.00-0.40	2.88 (3)	0.32		3 7.02		7 7.39			19 –	4 –
0.00-0.63	1.15 (4)	0.50			9 6.89			35 7.48		
0.00-1.00	4.57 (4)	0.79					44 6.98			
0.40-0.63	8.60 (3)	0.54		2 6.37		11 7.11			28 –	3 –
0.63-1.00	3.42 (4)	0.86		7 6.31	13 6.58	39 7.06		46 7.13	15 –	
1.00-1.59	1.36 (5)	1.36		10 5.87	27 6.30	45 6.52	80 6.77	24 6.25		
1.59-2.51	5.42 (5)	2.15	4 –	20 5.57	23 5.63	42 5.89	28 5.71			
2.51-3.98	2.16 (6)	3.40	4 –	19 4.94	20 4.97	14 4.81				
3.98-6.31	8.59 (6)	5.40	1 –	9 4.02	7 3.91					
		Total	9	70	99	158	152	105	62	7

Table 4: The logarithmic space density $D^* = \log D + 10$ for late-type giants (see text for definition of the symbols, distances in kpc, volumes in pc^3)

r_1-r_2	$\Delta V_{1,2}$	$\bar{r}$	N	D^*
0-3.98	2.88 (6)	3.16	10	4.54
3.98-6.31	8.60 (6)	5.40	16	4.27
6.31-10.00	3.42 (7)	8.55	5	3.16
10.00-19.95	3.17 (8)	16.48	6	$--$

Table 5: Local luminosity function resulting from comparison of observed histograms with best-fitting model gradients BRK, and confronted to Gliese's [17] and Hipparcos' (JW) local luminosity functions. s: standard deviation in units of logarithmic space density.

$M(G) \rightarrow$	(3-4]	(4-5]	(5-6]	(6-7]	(7-8]
BRK	6.91	7.12	7.48	7.55	7.77
$s(\pm)$	0.17	0.12	0.16	0.17	0.08
Gliese (1969)	7.18	7.41	7.52	7.48	7.42
Hipparcos (JW)	7.04	7.20	7.47	7.47	7.47